



Physical interpretations for cap parameters of the modified Drucker-Prager cap model in relation to the deviator stress curve of a particulate compact in conventional triaxial testing



Hyunho Shin ^{a,*}, Jong-Bong Kim ^{b,*}

^a Department of Materials Engineering, Gangneung-Wonju National University, 7 Jugheon-gil, Gangneung, Gangwon-do 210-702, Republic of Korea

^b Department of Mechanical and Automotive Engineering, Seoul National University of Science and Technology, 232 Gongneung-ro, Nowon-gu, Seoul 139-743, Republic of Korea

ARTICLE INFO

Article history:

Received 19 November 2014

Received in revised form 7 April 2015

Accepted 9 April 2015

Available online 17 April 2015

Keywords:

Modified Drucker-Prager cap model

Cap aspect ratio

Transition surface parameter

Deviator stress

ABSTRACT

The physical meanings of the cap aspect ratio (R) and transition surface parameter (α) of the modified Drucker-Prager cap (MDPC) model have been uncovered in relation to the deviator stress curves of a particulate material in conventional triaxial testing by simulating the curves using varying R and α based on finite element analysis. R controls the rate of the stress rise with the increase of the strain; the smaller the R , the faster the rise of the deviator stress. This phenomenon occurs because, in the p - q plane (p is the mean stress and q is the Mises equivalent stress), the cap with a smaller R needs to move a shorter distance on the p axis to maintain the current stress state: a smaller volumetric plastic strain is required according to the hardening law. R does not influence the maximum value of the deviator stress curve. As for the influence of α , it artificially lowers the true failure surface by an amount that is proportional to α so that a fictitious ultimate failure state is achieved. Therefore, it is desirable to set α as small as possible unless the numerical analysis using the MDPC model does not produce a converged solution. An analytical expression to calculate the maximum deviator stress that can be predicted by the MDPC model is provided in terms of α .

© 2015 Elsevier B.V. All rights reserved.

1. Introduction

In particulate materials, shear properties are the most important properties, while in the bulk metals and bulk ceramics, tensile and compressive properties, respectively, are the most important. Further, the particulate materials exhibit hydrostatic pressure-dependent yielding behavior. In order to describe such behavior of particulate materials precisely, a rigorous constitutive model together with its accurate parameters is a prerequisite. In this regard, the modified Drucker-Prager cap (MDPC) model has been employed extensively as the constitutive model [1–58] of the particulate materials in various engineering areas, especially in describing their compaction behavior. This model demonstrates a reliable prediction capability, especially when monotonic loading is involved. The input information for the MDPC model includes the parameters describing elastic behavior, the parameters defining the shear failure surface, the cap parameters (the cap aspect ratio, R , and the transition surface parameter, α) defining the shapes of the cap and the transition surface, and the hydrostatic pressure vs. the inelastic volumetric strain relationship governing the movement of the cap. Because many parameters are involved in the MDPC model, researchers investigated the sensitivity of the model parameters on the prediction result of

the model via a statistical or a parametric approach [56–58]. They found that the influences of the cap parameters (R and α) are the most significant among the material parameters of the MDPC model.

All of the required material parameters in the MDPC model, except the cap parameters, have straight-forward physical meanings as mentioned in Section 2, and they are determined suitably via experiment. It is difficult to assign cap parameters to any explicit properties of particulate materials and the experimental determination process is the most complicated among the model parameters. In the experimental determination process, the conventional triaxial test [59] is generally used to measure the deviator stress curves as functions of axial and radial strains at varying confinement pressures. Then, several series of iso-plastic-volumetric-strain data points are displayed in the meridional plane [35–37,60], from which R and α values are determined by non-linear curve fitting. Thus, the physical meanings of the determined cap parameters are fairly implicit. The parameter α is especially so because it was introduced in the MDPC model in order to ensure the stability in the numerical implementation.

Although the direct correlation of the cap parameters to the properties of particulate materials is difficult to establish due to the implicit nature of the parameters, if we investigate their roles in producing the deviator stress curves via a systematic simulation, their physical interpretations in relation to the important deviator stress curve may be found. Although, as mentioned, there has been some studies on the

* Corresponding authors. Tel.: +82 2 970 6434; fax: +82 2 979 7032.

E-mail addresses: hshin@gwnu.ac.kr (H. Shin), jbkim@seoultech.ac.kr (J.-B. Kim).

sensitivity of the cap parameters, they were carried out from the viewpoint of achieving the final density of the powder compact [56,57] or the axial stress [58], all of which are based on statistical analysis or on the range of the output of the MDPC model. Thus, one can hardly draw out the physics-based information on the roles of the cap parameters. Here we systematically simulate the deviator stress curves of the conventional triaxial test using varying cap parameters and explain why the observed influences of the parameters on the deviator stress curve are manifested based on the principle of the MDPC model. In particular, this study provides an analytical expression to calculate the maximum deviator stress as a function of one of the cap parameters, α .

2. Modified Drucker-Prager cap model

The modified Drucker-Prager cap (MDPC) model describes the yield surfaces in the p - q plane, where p is the mean stress (pressure) and q is the Mises-equivalent shear stress. Fig. 1 illustrates the model, which is adapted from the original reference [61] for the MDPC model. For the cylindrical specimen of the conventional triaxial test, q and p are given by

$$q = \sigma_a - \sigma_r = \sqrt{3}J_{2D} \quad (1)$$

$$p = \frac{\sigma_a + 2\sigma_r}{3} = \frac{J_1}{3} \quad (2)$$

where σ_a and σ_r are the axial and radial stresses, respectively. q is the deviator stress in the conventional triaxial test.

As illustrated in Fig. 1, there are three surfaces in the MDPC model: shear failure surface, cap, and the transition surface. This model adopts the Drucker-Prager shear failure surface [62], which reflects the pressure dependency of the yield surface:

$$f(p, q) = q - p \tan \beta - d = 0 \quad (3)$$

where $\tan \beta$ is the slope of the shear failure surface and d is the intercept of the q axis. β has the physical meaning of the internal friction angle of the particles. It is determined by the slope of the shear stress line in the shear stress-pressure domain of the failure surface and reflects the degree of interlocking and surface roughness of the particles. d is called the cohesion intercept which is the shear strength when the applied pressure is zero; it is the apparent cohesive strength of the particulate material itself when no external pressure is applied.

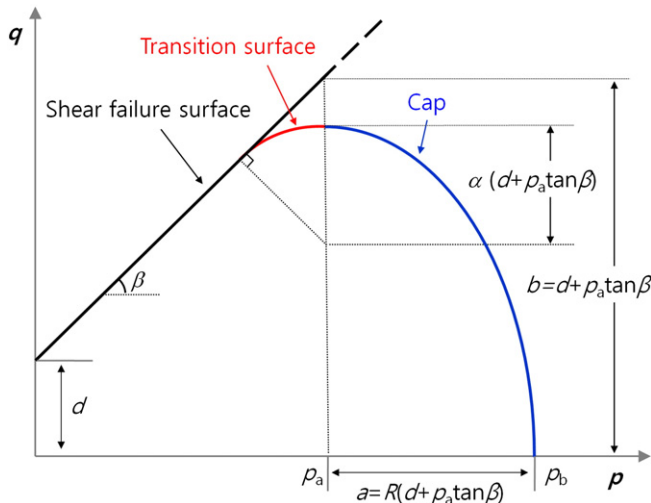


Fig. 1. Yield surfaces of the modified Drucker-Prager cap (MDPC) model in p - q plane. Adapted from the original reference [61] of the MDPC model.

The MDPC model employs a smooth transition surface between the shear failure surface and the cap in order to eliminate singularities in numerical implementation of the model, especially when the stress state moves from the cap surface to the failure surface. The transition surface is described by a small number α as follows [61]:

$$f(p, q, \varepsilon_v^p) = (p - p_a)^2 + [q - (1 - \alpha / \cos \beta)b]^2 - \alpha^2 b^2 = 0 \quad (4)$$

where p_a is the center of the cap on the hydrostatic axis, and α is the parameter related to the radius of the transition surface, as will be seen later.

The cap yield surface in the MDPC model is given by [61]:

$$f(p, q, \varepsilon_v^p) = (p - p_a)^2 + \left[\frac{Rq}{(1 + \alpha - \alpha / \cos \beta)} \right]^2 - R^2 b^2 = 0 \quad (5)$$

where ε_v^p is the plastic strain of the specimen that is determined by the inelastic (residual) strain when the specimen is unloaded from the hydrostatic pressure value of p_b , which is the cap position (intersection) on the hydrostatic pressure axis. $R (= a/b)$ is the ratio of the horizontal span of the cap on the hydrostatic axis to the original cap height (when the transition surface does not exist) and is called the cap aspect ratio. Since α controls not only the transition surface (Eq. (4)) but also the cap surface as seen in Eq. (5), α is called a cap parameter in this paper together with R that controls only the cap surface.

In the numerical implementation of the MDPC model, the direction of the plastic strain increment is normal to the plastic flow potential (flow rule). When the stress state is on the cap surface, the plastic flow potential function is identical to that of the cap surface (associated flow rule). On the shear failure surface and the transition surface, an elliptical flow potential function is used for both surfaces, which is different from the two yield surfaces (non-associated flow rule) [61]:

$$g(p, q, \varepsilon_v^p) = \sqrt{[(p - p_a) \tan \beta]^2 + [q / (1 + \alpha - \alpha / \cos \beta)]^2} \quad (6)$$

Explaining the operation principle of the MDPC model, the specimen behaves elastically when the stress state of the specimen is located in the volume surrounded by three surfaces. When the stress state of the specimen reaches the shear failure surface during the loading, the specimen fails by the shear action with no further change in shear stress or volume. The position of the cap (p_b) on the p axis is controlled by the hydrostatic pressure vs. inelastic volumetric strain relation (hardening law). Thus, the cap represents a locus of points with the same volumetric inelastic strain. When the stress state reaches the cap, it expands to define a new yield surface according to the hardening law, which allows additional plastic deformation after the yielding of the particulate materials (work hardening) prior to reaching the ultimate failure state defined by the failure surface. The stress state is on the surface of the moving cap during the plastic deformation because the stress state cannot be located beyond the yield surface. The moving cap also accounts for the plastic deformation under a pure hydrostatic loading. When the stress state reaches the failure surface that is located within the cap, the cap contracts toward the stress state on the failure surface. Then, the position of p_b decreases, which means, according to the hardening law, a decrease of the inelastic volume strain (i.e., the dilation of the particulate materials). The dilation ends when the contracting cap reaches the stress state on the failure surface.

In this study, we discuss all the terms (including material parameters) in the p - q plane following the definitions in the original reference [61] of the MDPC model. A positive sign is assigned to the compression.

3. Numerical analysis

For the numerical analysis of the constitutive behavior of the specimen in conventional triaxial test, a single cuboidal element (an eight node linear brick element) with a $25 \times 25 \times 25$ mm size was used

(Fig. 2). The nodes in the x-y plane were not allowed to move in the z direction (The x-y plane is the bottom surface of the cuboidal specimen and is the support plane for the specimen.). The movement of nodes in the y-z plane was fixed in the x direction and the nodes in the z-x plane were also the case in the y direction.

To simulate the hydrostatic loading stage in the conventional triaxial test, the same magnitude of pressure was applied to three visible surfaces of the cuboidal model shown in Fig. 2. For the subsequent shear loading stage, the z-displacement of nodes at the top surface of the model was controlled to achieve the shear state of the specimen.

The parameter set of the MDPC model used in this study (except for the cap parameters) is summarized in Table 1. According to Reference [52], the model parameters used in this study (Table 1 and the R value of 0.404) fit the triaxial deviator stress curves of a soil compact [63] at varying confinement pressures; conventional triaxial testing has been carried out most extensively for soils compared with any other particulate materials. In the numerical implementation of the MDPC model, the initial cap yield surface position on the hydrostatic pressure axis when the analysis begins is defined by the initial inelastic volume strain, $\varepsilon_v^{in}(0)$. It is the parameter indicating the degree of the initial compaction of the specimen. As the initial cap position increases, the pressure required to further compress the material increases (The required pressure is determined by the hardening law). In this study, $\varepsilon_v^{in}(0)$ was set to zero, which means that the specimen was initially consolidated to 47.381 kPa (See table 1) before starting the conventional triaxial test; the required pressure to initiate the isotropic (hydrostatic) plastic deformation is set to this pressure.

4. Results and discussion

4.1. Effect of R on the deviator stress curve

The deviator stress (q) curves of the conventional triaxial test were simulated at varying confinement pressures based on the MDPC model using varying values of R . Alpha was set to zero at all times to uncover the pure influence of R . Two examples of the simulated shear stress curves (when $R = 0.404$ and 0.289) are shown in Fig. 3(a). The R values of 0.404 and 0.289 in the p - q ($p - \sqrt{3}J_{2D}$) plane correspond to the R values of 0.7 and 0.5 in the $p - \sqrt{J_{2D}}$ plane. When the R value is smaller (0.289), the deviator stress rises faster with the strain at all of the investigated confinement pressures. As the axial strain increases sufficiently, however, there is no difference in the deviator stress regardless of the R value. Using the curves at 310 kPa shown in Fig. 3(a), the relative difference of q ($\Delta q/q$) was quantified and the result is shown in Fig. 3(b). As seen in Fig. 3(b), the relative difference of q is considerable (as high as approximately 0.17) when $\Delta R/R$ is -0.285 (= (0.289-0.404)/0.404).

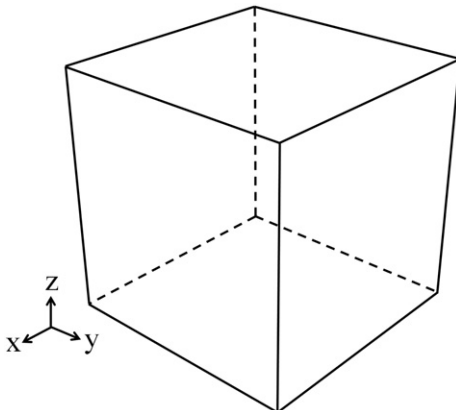


Fig. 2. Schematic illustration of the model for the finite element analysis.

Table 1

The parameter set of the MDPC model (in the q - p plane) used in this study. The cap parameters (R and α) were varied.

d (kPa)	β ($^\circ$)	E (MPa)	ν	Hardening law (kPa) ($x = \varepsilon_v^{in}$)
46.930	56.518	80	0.35	$p = 783, 694x^2 + 4, 302.8x + 47.381$

Comparing the load paths in the p - q domain for the two different simulation cases with different R values when $\alpha = 0$ (Fig. 4), there is no difference in the load path. Both cases reach the shear failure surface with a theoretical slope of 3 [64] during the shear loading stage. We also checked the influence of R on the deviator stress curve at nonzero values of α (not shown) and found that (1) a smaller R resulted in a faster rise of the deviator stress curve and (2) the maximum deviator stress was not influenced by R if the strain increased sufficiently (However, the maximum shear stress did not reach the failure surface when α was nonzero. This issue is treated in the next subsection.).

In order to understand the reason a reduced R value results in a faster rise of the deviator stress curve (and vice versa for an increased R), refer to Fig. 5, which compares the cap with a large R and a small R . In the hydrostatic loading stage of the conventional triaxial test, the stress state of the specimen moves from the origin to point p_0^* . In this stage, the current stress state lies on the pressure axis. Because the current stress state during plastic deformation is always on the cap, the

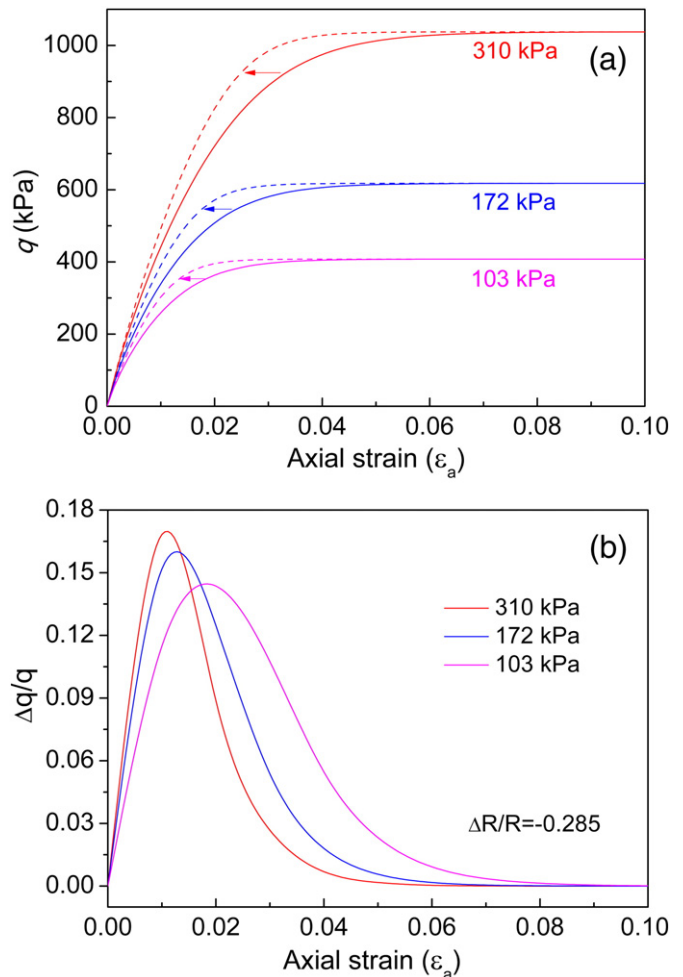


Fig. 3. (a) Curves of the deviator stress q at varying confinement pressures as a function of axial strain during the shear loading stage of the conventional triaxial test ($\alpha = 0$). Arrows indicate the direction of the curve shift at each confinement pressure as R decreases from 0.404 (solid curves) to 0.289 (dashed curves). (b) Plot for $\Delta q/q$.

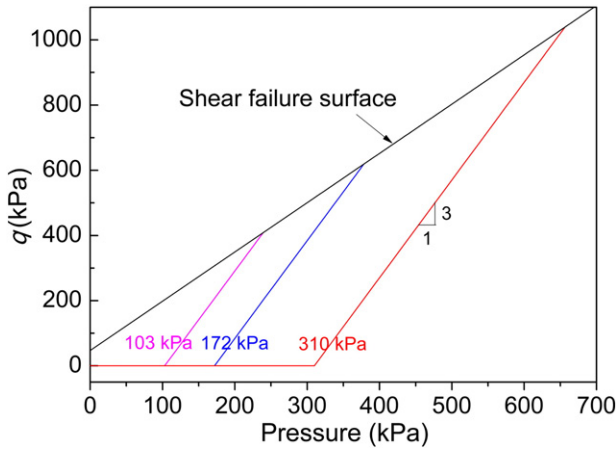


Fig. 4. Simulated load paths of the specimen at varying confinement pressures ($\alpha = 0$). The two simulated cases for $R = 0.289$ and 0.404 coincide.

current stress state is the intersection point between the cap and the pressure axis; the cap position (the intersection point) is the current stress state. Meanwhile the current stress state lies in the pressure axis, the cap position is the same for any caps with different R values, because, whatever R value the cap has, the position of any caps (intersection point) should describe the current stress state that lies in the pressure axis. An example is illustrated in Fig. 5 by dashed caps with different R values which are located at the same cap position (p_b^*).

As the shear loading stage starts in conventional triaxial testing, the current stress state offsets from the pressure axis (from point p_b^*) and moves along the load path with a slope of 3. At the beginning of the shear loading stage, as mentioned, the initial cap position is at p_b^* regardless of the magnitude of R . Now consider a current (p, q) state of the specimen during the shear loading stage (Fig. 5). The current (p, q) state (1) should follow the path with a slope of 3 and (2) is always on the cap because the stress state cannot be located outside of the yield surface. Therefore, the evolved shape of a large cap and that of a small cap at the current state (p, q) should be like the solid curves illustrated in Fig. 5. In this current stress state (p, q), the cap with a small R has moved out a shorter distance on the hydrostatic axis (to p_b^S) than the cap with a large R has done (p_b^L). This finding means that a smaller plastic volumetric strain (ϵ_v) has been evolved for the cap with the smaller R according to the hardening law. The evolution of a smaller ϵ_v

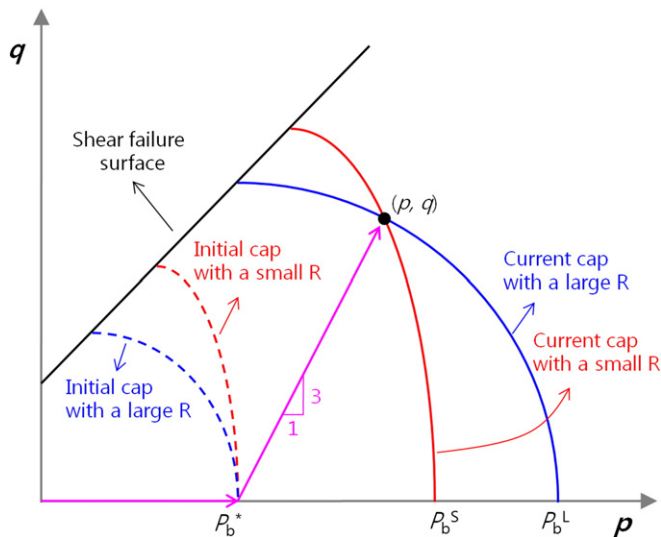


Fig. 5. Schematic illustration of the caps with two different R values at the current stress state (p, q) when α is zero.

at the current (p, q) state means the evolution of a smaller ϵ_a at the current values of p and q ($= 3p$), as illustrated in Fig. 6. In this figure, for a given value of q (current stress state), a smaller volumetric strain (a smaller axial strain) is evolved when R is smaller (0.289), which indicates that a smaller R value results in a faster rise of q in the q - ϵ_a domain (Fig. 3).

In Fig. 6, a given q value is achieved at a smaller ϵ_v (a smaller ϵ_a) when R is small. However, the same q value is certainly achieved later (at a larger ϵ_v and ϵ_a) when R is large. The only thing that matters for a larger R to achieve the ultimate (maximum) shear stress level is that the cap needs to move out further according to the hardening law (Fig. 5). Thus, the deviator stress q is the same eventually when the strain increases sufficiently regardless of the R value, which explains why R does not influence the maximum shear stress level that can be achieved in the specimen.

4.2. Effect of α on the deviator stress curve

The deviator stress curves of the conventional triaxial test were simulated at varying confinement pressures based on the MDPC model using varying values of α . R was set to 0.404 at all times to uncover the pure influence of α . Two examples of the simulated shear stress curves ($\alpha = 0$ and 0.1) are shown in Fig. 7. As seen in this figure, a larger α (solid curves) results in a diminished q value no matter how much the strain increases; the curve shifts downward as α increases. We also checked the influence of α on the deviator stress curve at other values of R (not shown) and found the same result. When α has a non zero value (e.g., 0.1), the investigation of the load path (Fig. 8) reveals that the stress state of the specimen does not reach the failure surface (It reaches the failure surface when $\alpha = 0$ regardless of the value of R as seen in Fig. 4). The final q values in Fig. 8 (the points at the end of each load path) are the same as the maximum q values of the corresponding solid curves ($\alpha = 0.1$) in Fig. 7. As the loading progresses (as the axial strain increases), the value of q (Fig. 7) as well as that of p ($= 1/3q$) is saturated, thereby resulting in an asymptotic approach of the current stress state toward the final (p, q) point located at the end of each load path in Fig. 8.

In order to understand why an increased α value results in a diminished maximum deviator stress (Figs. 7 and 8), we revisited the MDPC model shown in Fig. 1 (adapted from the original reference of the MPDPC model) and interpreted the model as illustrated in Fig. 9. In Fig. 9(a), the transition surface (in red) is a right circle with the radius r ($= \alpha b$) where α is the ratio of the radius of the transition surface (r)

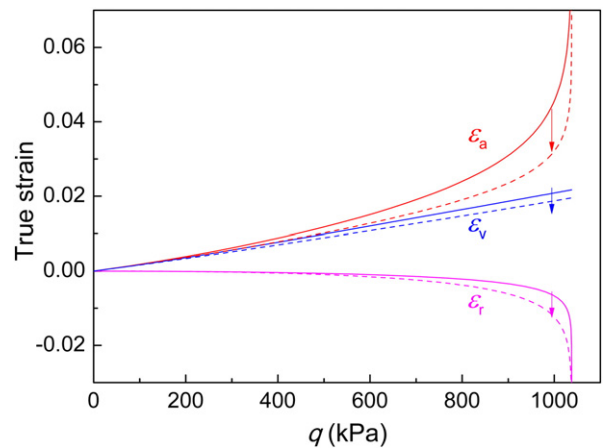


Fig. 6. The profiles of axial (ϵ_a), radial ($\epsilon_r = \epsilon_x = \epsilon_y$), and volumetric ($\epsilon_v = \epsilon_a + 2\epsilon_r$) strains at the confinement pressure of 310 kPa as functions of q ($\alpha = 0$). The arrows indicate the decrease of the respective strains as R decreases from 0.404 (solid curves) to 0.289 (dashed curves). Because the signs of ϵ_a and ϵ_r are different, the change in ϵ_v is less significant than that of ϵ_a or ϵ_r .

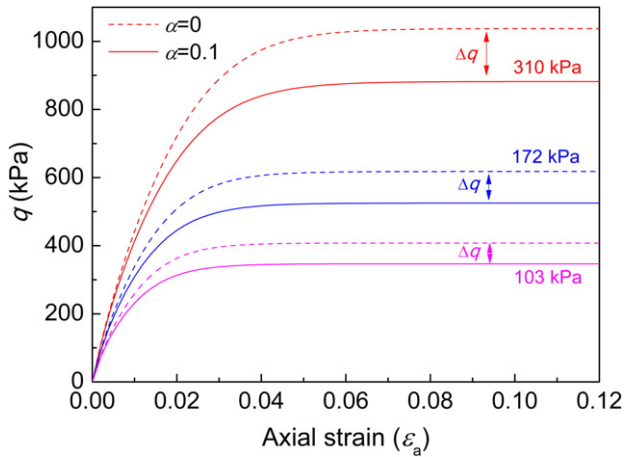


Fig. 7. Curves of the deviator stress $q (= \sigma_a - \sigma_r)$ at varying confinement pressures as a function of axial strain during the shear loading stage of the conventional triaxial test ($R = 0.404$). Arrows indicate the amount of the curve shift at each confinement pressure between the α values of 0 (dashed curves) and 0.1 (solid curves).

to the height of the original cap when α is zero: $\alpha = r/b$ (See Appendix A). The transition surface can be considered to start from the point m on the vertical line $i-p_a$ toward the shear failure surface (point j): the length of the arc is $\alpha\beta b$ (β in radian). Then, the original cap surface is modified in the MDPC model by squeezing the original cap along the vertical direction until the top of the original cap meets the point m . (The reason why we interpret the modified cap surface in this way is provided in Appendix A.) Then, the decrease of the cap height is proportional to α as qualitatively seen in Fig. 9(b). The degree of squeeze of the modified cap surface along the vertical direction is proportional to α : the larger the α , the larger the degree of the modification (squeezing) of the original cap.

As seen in Fig. 9(a), the intersection between the transition surface and the cap surface (point m) is the maximum point of the two surfaces. With this finding in mind, refer to Fig. 10 which shows the caps located at varying positions; at the initial state of the load path in the shear stage (noted by superscript o), at the intermediate state (superscript i), and at the state when the stress state on the load path reaches the maximum point (superscript m). As the stress state (p, q) follows the load path with a slope of 3, the position on the cap surface (the current stress state) moves up along the cap. When the current stress state reaches point m , the cap cannot move out further because (1) point m is the maximally allowable q value on the cap and the transition surfaces at the current volumetric strain (corresponding to p^m) and (2) any further

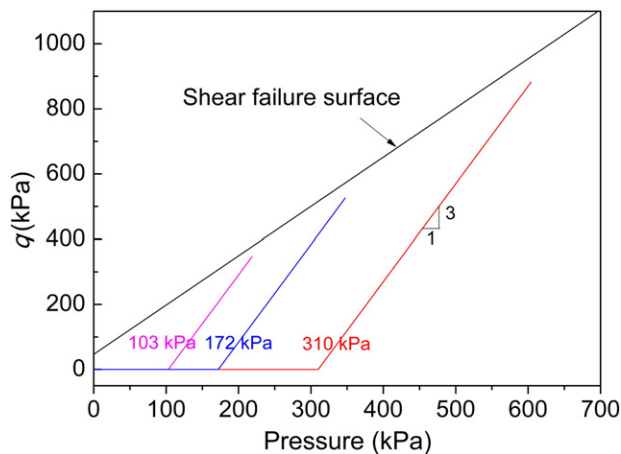


Fig. 8. Simulated load paths of the specimen at varying confinement pressures when α is 0.1 ($R = 0.404$).

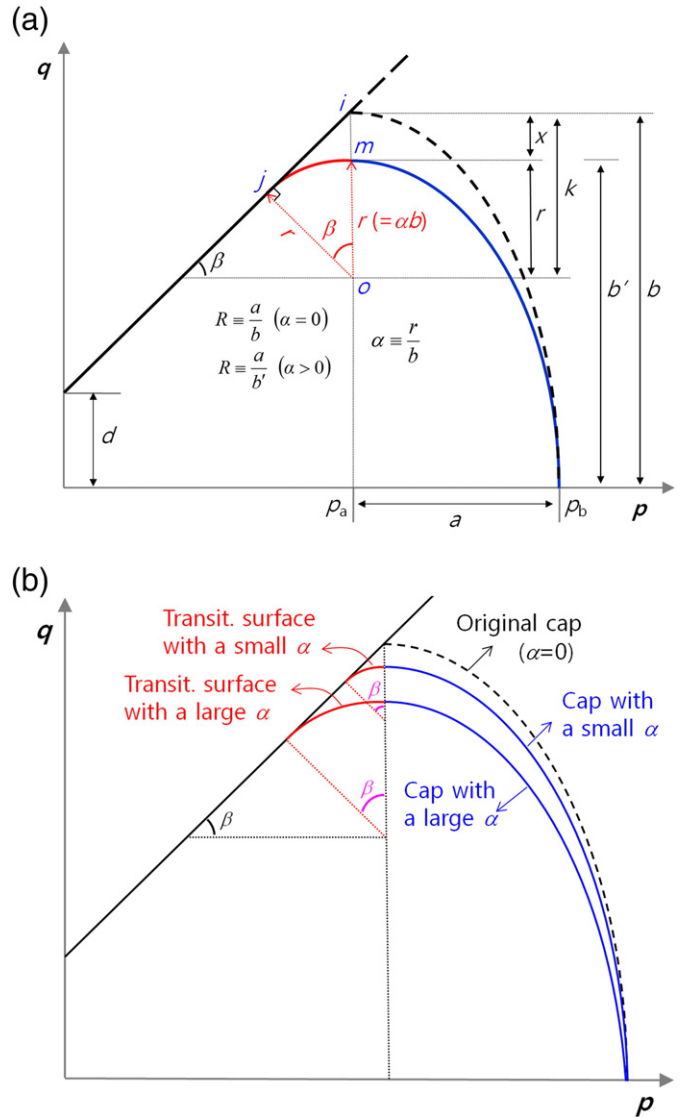


Fig. 9. Interpretation of the MDPC model (a) for a given α and (b) for two different values of α .

progress of the stress state should follow the load path with the slope of 3. Therefore, the stress state of the specimen is fixed at the maximum point m (p^m, q^m). This reasoning is consistent with the fact that the profiles of the volumetric strain and pressure are saturated with the progress of the axial displacement (Fig. 11). In Fig. 11, when α increases from 0 to 0.1, the saturation values of ϵ_v (and subsequently p) decrease, together with the decreased q value when α increases (Fig. 7): The (p, q) state never reaches the shear failure surface. Although the saturation values of q 's are α -dependent, once they reach their maximal values, they vary no longer in spite of the progress of the axial strain; the stress state in the p - q domain is fixed (point m in Fig. 10).

When $\alpha > 0$, it can be said that the saturated stress state (where q is maximum) reaches a new ultimate failure state in that there is no change in shear stress (Fig. 7) or volume (Fig. 11) [65] in the saturated stress state. Therefore, α artificially lowers the true (original) failure surface defined by d and $\tan\beta$ by the amount that is proportional to α so that a fictitious ultimate failure state is achieved. When α is overly large, the moving part of the yield surface is the combination of a large circle (the transition surface) with a significantly squeezed ellipse (the cap in Fig. 9(b)), which causes the problem of lowering the ultimate failure state excessively. In the framework of the MDPC model, the shape of locus of the iso-inelastic-volume strain in the p - q domain

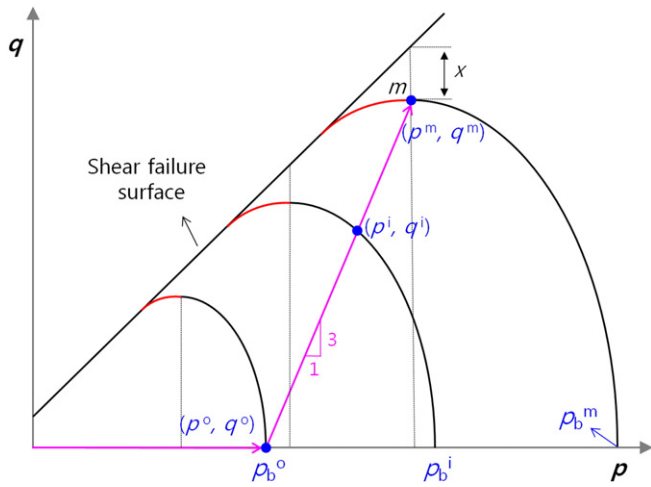


Fig. 10. Schematic illustration of the caps located at varying positions; at the initial state of load path in the shear stage, at the intermediate state, and at the state when the stress state following the load path reaches the maximum point.

(the shape of the cap surface) should be described solely by the change in R because the description of the cap shape by way of setting a non-zero valued α ($\alpha > 0$) artificially lowers the yield surface. This finding suggests that, when we experimentally determine the cap parameters of a given particulate material, it is desirable to obtain the R value by setting the value of α as zero. Recall that α was introduced to the MDPC model simply to impose a numerical stability. It is not a material constant.

Ref. [36] experimentally obtained R with an overly large α ($\alpha = 0.224$ or 2.776). In this reference, the set of R and α was determined simultaneously from the non-linear fitting of all available sets of iso-elastic-volume-strain loci. If R was determined by setting the value of α as zero, the value of R could be determined for each set of the iso-elastic-volume-strain locus, which could reveal the evolution of R as a function of the inelastic volumetric strain.

In numerical analysis, it is desirable to set α as small as possible unless the numerical analysis using the MDPC model does not produce a converged solution. The user of the model may set a non-zero value of α from the viewpoint of apparently fitting an engineering event. If the engineering event of interest is simulated successfully with only an overly large α , it results from the numerical fiction of the model (the limitation of the model) because α renders the model not to reach the true failure surface of the material.

We now seek an analytical expression to calculate the maximum deviator stress. In Fig. 12, q values of point f (q^f) and point m (q^m) are

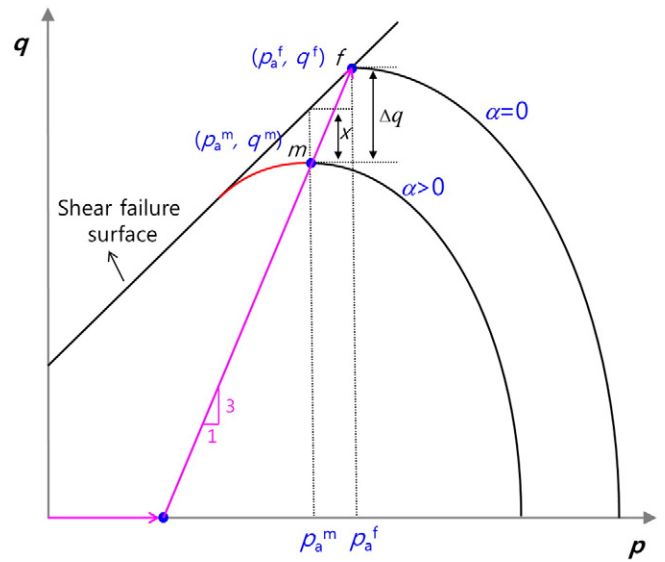


Fig. 12. Definition of Δq (the difference of the maximum deviator stress between the cases of $\alpha = 0$ and $\alpha > 0$) in the p - q domain.

maximum deviator stresses when $\alpha = 0$ and $\alpha > 0$, respectively. In Fig. 7, the difference of the maximum deviator stress between the cases of $\alpha = 0$ and $\alpha > 0$ is noted as Δq . Δq can be defined in the p - q domain as seen in Fig. 12.

Based on the process shown in Appendix B, q^m is expressed as follows:

$$q^m = \frac{3(zd + 3c)}{3 - z \tan \beta} - 3c \quad (7)$$

where c is the confinement pressure and z is the ratio of the height (b') of the modified cap to that (b) of the original cap (See Fig. 9(a)). z is given as a function of α by

$$z \equiv \frac{b'}{b} = 1 + \alpha - \frac{\alpha}{\cos \beta} \quad (8)$$

When $z = 1$ ($\alpha = 0$), Eq. (7) predicts the value of q^f (See Fig. 12.). In this case, Eq. (7) predicts q^f values of 408.5, 618.8, and 1039.4 kPa for the confinement pressures of 103, 172, and 310 kPa, respectively. When α is 0.1 ($z = 0.919$), q^m values predicted by Eq. (7) are 346.7, 525.2, and 882.1 kPa, respectively. All of these calculated values by Eq. (7) are identical to the maximum (saturated) q values numerically obtained in Fig. 7 at respective confinement pressures. From this finding, the validity of the analytical expression (Eq. (7)) is confirmed.

4.3. Mixed influence of R and α on the deviator stress curve

When we simulated the cases with varied R and α simultaneously (not shown), the influences of R and α operated independently. Thus, the individual findings (described in the previous subsections) on the influence of R and that of α on the shear stress curve are generally applied for arbitrary sets of R and α . The findings on the influence of R on the deviator stress of the conventional triaxial test may be applied to other types of the cap models such as the geologic cap model [66] and the continuous surface cap model [66,67]. In the continuous surface cap model, the shape of the transition surface is different from that of the MDPC model, while it is noted that there is also a maximum point in the moving part of the yield surface like the case of the MDPC model.

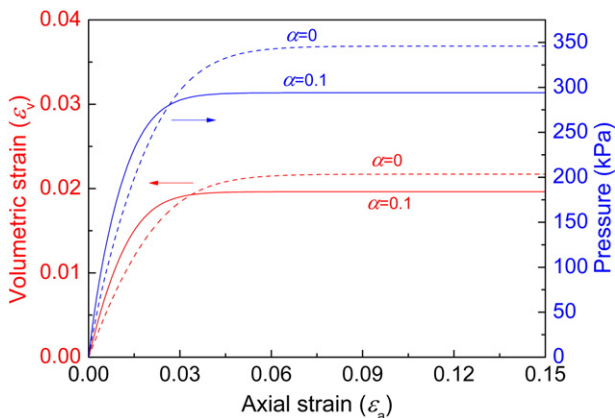


Fig. 11. Change in the volumetric strain and pressure as functions of axial strain for the confinement pressure of 310 kPa ($R = 0.404$).

5. Conclusion

The physical meanings of the cap parameters (the cap aspect ratio, R , and transition surface parameter, α) of the modified Drucker-Prager cap (MDPC) model have been uncovered in relation to the deviator stress curves of particulate materials in conventional triaxial testing by simulating the curves using varying R and α based on the finite element analysis. R controls the rate of rise of the deviator stress with the increase of the strain; the smaller the R , the faster the rise of the deviator stress. This phenomenon occurs because, in the p - q space, the cap with a smaller R needs to move a shorter distance on the p axis to maintain the current stress state: a less plastic volumetric strain is required according to the hardening law. R does not influence the maximum value on the deviator stress curve of the specimen; the only thing that matters for the larger R is that the cap needs to move out further (a further plastic volumetric strain is required) for the specimen to reach the maximum deviator stress. As for the influence of α , it artificially lowers the true failure surface by the amount that is proportional to α so that a fictitious ultimate failure state is achieved. Therefore, when we experimentally determine the cap parameters of a given particulate material, it is desirable to obtain the R value by setting the value of α as zero. In numerical analysis, it is desirable to set α as small as possible unless the numerical analysis using the MDPC model does not produce a converged solution. If an engineering event of interest is simulated successfully with only an overly large α , it results from the numerical fiction of the model (the limitation of the model) because α renders the model not to reach the true failure surface of the material. An analytical expression to calculate the maximum deviator stress is provided in terms of the parameters of α and the true failure surface. The influence of R and that of α operate independently so that the individual findings on the influence of R and that of α on the deviator stress curve are generally applied for arbitrary sets of R and α .

Acknowledgments

This study was financially supported by the Ministry of Education, Science, and Technology through the National Research Foundation (NRF) of Korea under contract No. 2013R1A1A2007455.

Appendix A

This appendix explains (1) the right-circular nature of the transition surface and (2) the reason the modified cap (when $\alpha > 0$) in the modified Drucker-Prager cap model is interpreted to be squeezed from the original cap along the vertical direction. In Fig. 9(a), b is the height of the original cap when α is zero. The height of the modified cap is noted as b' .

From the consideration of the rectangular triangle Δijo shown in Fig. 9(a), we find the relation:

$$k \cos \beta = \alpha b \quad (\text{A1})$$

Then, the vertical coordinate of point O (q^0) is

$$q^0 = b - k = b \left(1 - \frac{\alpha}{\cos \beta} \right) \quad (\text{A2})$$

If the right circle with radius $r (= \alpha b)$ is shifted from the origin to the point O (p_a, q^0), the function of the circle will be

$$(p - p_a)^2 + [q - (1 - \alpha / \cos \beta)b]^2 - \alpha^2 b^2 = 0 \quad (\text{A3})$$

which is identical to the transition surface function of the MDPC model (Eq. (4)). Thus, the transition surface is a right circle with radius $r (= \alpha b)$ located at the point O.

The gap between the shear failure surface and the maximally allowable q value of the specimen is noted as x (Fig. 9(b)), which means that

$$b' = b - x \quad (\text{A4})$$

The gap x is given by

$$x = k - \alpha b = \alpha b \left(\frac{1}{\cos \beta} - 1 \right) \quad (\text{A5})$$

The height ratio of the modified and original cap (z) is expressed as

$$z \equiv \frac{b'}{b} = \frac{b - x}{b} = 1 - \frac{x}{b} \quad (\text{A6})$$

By plugging Eq. (A5) into (A6),

$$z = 1 + \alpha - \frac{\alpha}{\cos \beta} \quad (\text{A7})$$

This term (the height ratio of the caps) is found in the cap function (Eq. (5)) and the flow potential function (Eq. (6)). If we plug Eq. (A7) into the definition of z , which is $b' = bz$,

$$b' = b \left(1 + \alpha - \frac{\alpha}{\cos \beta} \right) \quad (\text{A8})$$

If the modified cap were constructed by squeezing the original cap along the vertical direction to form a new type of ellipse, the following ellipse relation should hold:

$$\frac{(p - p_a)^2}{R^2 b^2} + \frac{q^2}{b'^2} = 1 \quad (\text{A9})$$

Substituting Eq. (A8) for b' in Eq. (A9) leads to

$$(p - p_a)^2 + \frac{R^2 q^2}{(1 + \alpha - \alpha / \cos \beta)^2} = R^2 b^2 \quad (\text{A10})$$

Eq. (A10) is identical to the cap function (Eq. (5)). Thus, the modified cap ($\alpha > 0$) in the MDPC model turns out to be constructed by squeezing the original cap ($\alpha = 0$) along the vertical direction by the amount of x given by Eq. (A5) or by the height ratio of the caps with z (Eq. (A7)).

Appendix B

In order to calculate q^f and q^m shown in Fig. 12, we first seek p_a^m and p_a^f , respectively. Note that, from the knowledge of the slope of the load path, the load path function is

$$q = 3(p - c) \quad (\text{B1})$$

where c is the confinement pressure.

p_a^f is obtained by equating the load path function (Eq. (B1)) with the shear failure surface function (Eq. (3)):

$$p_a^f = \frac{d + 3c}{3 - \tan \beta} \quad (\text{B2})$$

Subsequently q^f is obtained by substituting Eq. (B2) for Eq. (B1):

$$q^f = 3 \left(\frac{d + 3c}{3 - \tan \beta} - c \right) = \frac{3(d + c \tan \beta)}{3 - \tan \beta} \quad (\text{B3})$$

For the expression of q^m , as mentioned, p_a^m is first obtained by equating the load path function (Eq. (B1)) with the cap function (Eq. (5)):

$$(p-p_a)^2 + \frac{R^2 q^2}{z^2} = R^2 b^2 \quad (\text{B4})$$

By plugging Eq. (B1) into Eq. (B4),

$$(p-p_a)^2 + \frac{9R^2(p-c)^2}{z^2} = R^2 b^2 \quad (\text{B5})$$

When $p = p_a = p_a^m$, Eq. (B5) transforms to

$$9(p_a^m - c)^2 = z^2 b^2 \quad (\text{B6})$$

which yields the relation

$$p_a^m = \frac{1}{3}zb + c \quad (\text{B7})$$

By noting that $b = a/R$, and a is given by $(d + p_a^m \tan \beta)R$, Eq. (B7) transforms to

$$p_a^m = \frac{zd + 3c}{3 - z \tan \beta} \quad (\text{B8})$$

Plugging Eq. (B8) to Eq. (B1) yields q^m as

$$q^m = \frac{3(zd + 3c)}{3 - z \tan \beta} - 3c \quad (\text{B9})$$

When $z = 1$ ($\alpha = 0$), Eq. (B9) becomes Eq. (B3). From Eqs. (B3) and (B9), Δq shown in Fig. 12 is expressed as follows:

$$\Delta q \equiv q^f - q^m = \frac{3(d + c \tan \beta)}{3 - \tan \beta} - \frac{3(zd + 3c)}{3 - z \tan \beta} + 3c \quad (\text{B10})$$

References

- [1] I. Aydin, B.J. Briscoe, K.Y. Şanhtürk, The internal form of compacted ceramic components: a comparison of a finite element modelling with experiment, *Powder Technol.* 89 (1996) 239–254.
- [2] I. Aydin, B.J. Briscoe, K.Y. Şanhtürk, Dimensional variation of die-pressed ceramic green compacts: comparison of a finite element modelling with experiment, *J. Eur. Ceram. Soc.* 17 (1997) 1201–1212.
- [3] A. Michrafy, D. Ringenbacher, P. Tchoreloff, Modelling the compaction behaviour of powders: application to pharmaceutical powders, *Powder Technol.* 127 (2002) 257–266.
- [4] A. Michrafy, H. Diarra, J.A. Dodds, M. Michrafy, L. Penazzi, Analysis of strain stress state in roller compaction process, *Powder Technol.* 208 (2011) 417–422.
- [5] C.-Y. Wu, O.M. Ruddy, A.C. Bentham, B.C. Hancock, S.M. Best, J.A. Elliott, Modelling the mechanical behaviour of pharmaceutical powders during compaction, *Powder Technol.* 152 (2005) 107–117.
- [6] C.-Y. Wu, B.C. Hancock, A. Mills, A.C. Bentham, S.M. Best, J.A. Elliott, Numerical and experimental investigation of capping mechanisms during pharmaceutical tablet compaction, *Powder Technol.* 181 (2008) 121–129.
- [7] L.H. Han, J.A. Elliott, A.C. Bentham, A. Mills, G.E. Amidon, B.C. Hancock, A modified Drucker-Prager Cap model for die compaction simulation of pharmaceutical powders, *Int. J. Solids Struct.* 45 (2008) 3088–3106.
- [8] L.H. Han, J. Elliott, S. Best, R. Cameron, A.C. Bentham, A. Mills, G.E. Amidon, B.C. Hancock, Numerical simulation on pharmaceutical powder compaction, *Mater. Sci. Forum* 575–578 (2008) 560–565.
- [9] L.H. Han, P.R. Laity, R.E. Cameron, J.A. Elliott, Density and plastic strain evaluations using small-angle X-ray scattering and finite element simulations for powder compacts of complex shape, *J. Mater. Sci.* 46 (2011) 5977–5990.
- [10] I.C. Sinka, J.C. Cunningham, A. Zavaliangos, Analysis of tablet compaction. II. Finite element analysis of density distributions in convex tablets, *J. Pharm. Sci.* 93 (8) (2004) 2040–2052.
- [11] J.C. Cunningham, I.C. Sinka, A. Zavaliangos, Analysis of tablet compaction. I. Characterization of mechanical behavior of powder and powder/tooling friction, *J. Pharm. Sci.* 93 (8) (2004) 2022–2039.
- [12] I.C. Sinka, Modelling Powder Compaction, *KONA* 25 (2007) 4–22.
- [13] I.C. Sinka, J.C. Cunningham, A. Zavaliangos, The effect of wall friction in the compaction of pharmaceutical tablets with curved faces: a validation study of the Drucker-Prager Cap model, *Powder Technol.* 133 (2003) 33–44.
- [14] C. Shang, I.C. Sinka, J. Pan, Constitutive model calibration for powder compaction using instrumented die testing, *Exp. Mech.* 52 (2012) 903–916.
- [15] H. Zipse, Finite-element simulation of the die pressing and sintering of a ceramic component, *J. Eur. Ceram. Soc.* 17 (1997) 1707–1713.
- [16] P. Chen, G.Y. Kim, J. Ni, Investigations in the compaction and sintering of large ceramic parts, *J. Mater. Process. Technol.* 190 (2007) 243–250.
- [17] W. Chen, Y. Yamamoto, W.H. Peter, S.B. Gorti, A.S. Sabau, M.B. Clark, S.D. Nunn, J.O. Kiggans, C.A. Blue, J.C. Williams, B. Fuller, K. Akhtar, Cold compaction study of Armstrong Process® Ti–6Al–4 V powders, *Powder Technol.* 214 (2011) 194–199.
- [18] O.G. Abdullah, F.A. Rasin, T.A. Al-Dhahir, Simulation study for the ceramic powder compaction process, *J. KUFA-Phys.* 1 (2009) 12–24.
- [19] O.G. Abdullah, F.A. Rasin, T.A. Al-Dhahir, Finite element simulation of alumina ceramic powder compaction, *Int. J. Pure Appl. Phys.* 5 (2009) 15–31.
- [20] R.Z. Moayed, S. Tamassoki, E. Izadi, Numerical modeling of direct shear tests on sandy clay, *World Acad. Sci. Eng. Technol.* 6 (2012) 939–943.
- [21] R. Zhou, L.-h. Zhang, B.-y. He, Y.-h. Liu, Numerical simulation of residual stress field in green power metallurgy compacts by modified Drucker – Prager Cap model, *Trans. Nonferrous Metals Soc. China* 23 (2013) 2374–2382.
- [22] G. Si, L. Chen, H. Shi, Y. Xie, R. Heng, Finite element analysis of pharmaceutical powder compaction with modified Drucker-Prager cap model, *Chin. J. Pharm.* 44 (2013) 88–94.
- [23] G.N. Si, L. Chen, Finite element analysis of pharmaceutical tablet compaction, *Appl. Mech. Mater.* 217–219 (2012) 2117–2120.
- [24] Y.Y. Foo, Y. Sheng, B.J. Briscoe, An experimental and numerical study of the compaction of alumina agglomerates, *Int. J. Solids Struct.* 41 (2004) 5929–5943.
- [25] Y.-B. Kim, J. Lee, S. Lee, H.-J. Park, G.-A. Lee, Calibration of a density-dependent modified Drucker-Prager cap model for AZO powder, *Adv. Mater. Res.* 482–484 (2012) 1249–1256.
- [26] J. Lee, Y.-B. Kim, S. Lee, J.-H. Song, J.-S. Park, G.-A. Lee, A density-dependent modified Drucker-Prager cap model of indium tin oxide powder, *Adv. Sci. Lett.* 15 (2012) 281–284.
- [27] P.M. Modnet, Comparison of computer models representing powder compaction process, *Powder Metall.* 42 (1999) 301–311.
- [28] T. Sinha, J.S. Curtis, B.C. Hancock, C. Wassgren, A study on the sensitivity of Drucker-Prager Cap model parameters during the decompression phase of powder compaction simulations, *Powder Technol.* 198 (2010) 315–324.
- [29] T. Sinha, R. Bharadwaj, J.S. Curtis, B.C. Hancock, C. Wassgren, Finite element analysis of pharmaceutical tablet compaction using a density dependent material plasticity model, *Powder Technol.* 202 (2010) 46–54.
- [30] O. Coube, H. Riedel, Numerical simulation of metal powder die compaction with special consideration of cracking, *Powder Metall.* 43 (2000) 123–131.
- [31] T. Kraft, H. Riedel, O. Rosenfelder, Compaction and sintering of a ceramic seal: modeling and experimental response, *Int. J. Powder Metall.* 39 (2003) 27–34.
- [32] T. Kraft, Optimizing press tool shapes by numerical simulation of compaction and sintering-application to hard metal cutting insert, *Model. Simul. Mater. Sci. Eng.* 11 (2003) 381–400.
- [33] T. Kraft, H. Riedel, P. Stingl, F. Wittig, Finite element simulation of die pressing and sintering, *Adv. Eng. Mater.* 1 (1999) 107–109.
- [34] J.-D. Prigge, K. Sommer, Numerical investigation of stress distribution during die compaction of food powders, *Part. Sci. Technol.* 29 (2011) 40–52.
- [35] K.T. Kim, S.W. Choi, H. Park, Densification behavior of ceramic powder under cold compaction, *Trans. ASME* 122 (2000) 238–244.
- [36] D.H. Zeuch, J.M. Graziar, J.G. Argüello, K.G. Ewsuk, Mechanical properties and shear failure surfaces for two alumina powders in triaxial compression, *J. Mater. Sci.* 36 (2001) 2911–2924.
- [37] S.C. Lee, K.T. Kim, Densification behavior of aluminum alloy powder under cold compaction, *Int. J. Mech. Sci.* 44 (2002) 1295–1308.
- [38] D. Volik, Evaluation of stamps and latex shell influence on stabilometer testing results - modeled with Simulia Abaqus, *Int. J. GEOMATE* 1 (2011) 135–139.
- [39] M.Y. Fattah, M.J. Al-Mosawi, A.A.O. Al-Zayadi, Time dependent behavior of piled raft foundation in clayey soil, *Geomech. Eng.* 5 (2013) 17–36.
- [40] A. Azimi, J. K’ovecses, J. Angeles, Wheel-soil interaction model for rover simulation and analysis using elastoplasticity theory, *IEEE Trans. Robot.* 29 (2013) 1271–1288.
- [41] B.M. Luccioni, M. Luege, Concrete pavement slab under blast loads, *Int. J. Impact Eng.* 32 (2006) 1248–1266.
- [42] E. Stilger-Szydlo, W. Tutaj, Effect of mining deformations on stability of transport embankments, *Stud. Geotech. Mech.* 26 (2004) 3–22.
- [43] R.C. Chiroux, W.A. Foster Jr., C.E. Johnson, S.A. Shoop, R.L. Raper, Three-dimensional finite element analysis of soil interaction with a rigid wheel, *Appl. Math. Comput.* 162 (2005) 707–722.
- [44] L.-H. Ho, C.-C. Hsieh, Numerical modeling for undrained shear strength of clays subjected to different plasticity indexes, *J. GeoEng.* 8 (3) (2013) 91–100.
- [45] L. Hua, W. Junjiao, H. Tianyou, M. Hiroyasu, A new numerical simulation model for high pressure squeezing moulding, *China Foundry* 8 (2011) 25–29.
- [46] H. Diarra, V. Mazel, V. Busignies, P. Tchoreloff, FEM simulation of the die compaction of pharmaceutical products: Influence of visco-elastic phenomena and comparison with experiments, *Int. J. Pharm.* 453 (2013) 389–394.
- [47] H. Diarra, V. Mazel, A. Boillon, L. Rehaut, V. Busignies, S. Bureau, P. Tchoreloff, Finite Element Method (FEM) modeling of the powder compaction of cosmetic products: Comparison between simulated and experimental results, *Powder Technol.* 224 (2012) 233–240.
- [48] G. Frenning, Analysis of pharmaceutical powder compaction using multiplicative hyperelasto-plastic theory, *Powder Technol.* 172 (2007) 103–112.
- [49] B. Zhang, M. Jain, C. Zhao, M. Bruhis, R. Lawcock, K. Ly, Experimental calibration of density-dependent modified Drucker-Prager/Cap model using an instrumented cubic die for powder compact, *Powder Technol.* 204 (2010) 27–41.

- [50] A. Zavaliangos, S. Galen, J. Cunningham, D. Winstead, Temperature evolution during the compaction of pharmaceutical powders, *J. Pharm. Sci.* 97 (2008) 3291–3304.
- [51] G. Klinzing, A. Zavaliangos, J. Cunningham, T. Mascaro, D. Winstead, Temperature and density evolution during compaction of a capsule shaped tablet, *Comput. Chem. Eng.* 34 (2010) 1082–1091.
- [52] H. Shin, J.-B. Kim, S.-J. Kim, K.Y. Lee, A simulation-based determination of cap parameters of the modified Drucker-Prager cap model by considering specimen barreling during conventional triaxial testing, *Comput. Mater. Sci.* 100 (2015) 31–38.
- [53] C. Lu, Determination of Cap Model Parameters using Numerical Optimization Method for Powder Compaction (Ph.D. Thesis) Marquette University, 2009.
- [54] G. Waggle, Die Compaction Simulation: Simplifying the Application of a Complex Constitutive Model Using Numerical and Physical Experiments (Ph.D. Thesis) The Pennsylvania State University, 2006.
- [55] S. Helwany, Applied Soil Mechanics with ABAQUS Applications, John Wiley and Sons, Inc., Hoboken, 2007. 61–67.
- [56] Y. He, R.S. Engel, N.J. Salamon, R. Zhang, Sensitivity study and parameter determination for 316 L stainless steel powder die compaction, *Proc. 2002 International Conference on Process Modeling in Powder Metallurgy (Process modeling in powder metallurgy & particulate materials)* 2002, pp. 99–106.
- [57] G.S. Waggle, R.S. Engel, R. Bollina, R.M. German, Statistical analysis of modified Drucker-Prager cap model parameters for applications to modeling die compaction, *Proceedings of the 2003 International Conference on Powder Metallurgy & Particulate Materials, Part IV* 2003, pp. 24–36.
- [58] M.P. Ayers, S.E. Clift, S. Gheduzzi, Prediction of subsidence in impaction grafting: a sensitivity analysis using the Taguchi method, 6th World Congress of Biomechanics, 1–6 August 2010, Singapore, IFMBE Proceedings, 31 2010, pp. 612–615.
- [59] J.P. Bardet, *Experimental Soil Mechanics*, Prentice Hall, Upper Saddle River (NJ), 1997. 443–469.
- [60] H.G. Kim, O. Gillia, P. Dorémus, D. Bouvard, Near net shape processing of a sintered alumina component: adjustment of pressing parameters through finite element simulation, *Int. J. Mech. Sci.* 44 (2002) 2523–2539.
- [61] Dassault Systèmes Simulia Corp., ABAQUS Theory Manual 6.13, 2013.
- [62] D.C. Drucker, W. Prager, Soil mechanics and plastic analysis for limit design, *Q. Appl. Math.* 10 (1952) 157–165.
- [63] K.Z.Z. Lee, N.-Y. Chang, K.T. Chang, Determination of cap model parameters using drained conventional triaxial compression test results, *Modernization and Optimization of Existing Dams and Reservoirs 2007*, pp. 275–284 (27th Annual USSD Conference, Philadelphia, Pennsylvania, March 5–9, 2007; U.S. Army Corps of Engineers).
- [64] W.-F. Chen, *Constitutive Equations for Engineering Materials, Vol. 2*, Elsevier, New York, 1994. 1014.
- [65] J.A. Knappett, R.F. Craig, *Craig's Soil Mechanics*, 8th Ed. Spon Press, London, 2012. 169.
- [66] Livermore Software Technology Corp., LS-DYNA Keyword User's Manual, Vol. II, Material Models, 2012.
- [67] L.E. Schwer, Y.D. Murray, Continuous surface cap model for geomaterial modeling: A new LS-DYNA material type, 7th Int. LS-DYNA User's Conference, 2009 (pp. 16–35–16–50).